Carbon doping controlled thermoluminescent defect centers in nanoporous alumina for ion beam dosimetry

S. Bhowmick, S. Pal, D. Das, V. K. Singh, S. A. Khan, R. Hübner, S. R. Barman, D. Kanjilal, and A. Kanjilal

Articles you may be interested in

Defect-engineered optical bandgap in self-assembled TiO_2 nanorods on Si pyramids
Applied Physics Letters **108**, 011907 (2016); 10.1063/1.4939662

Oxygen mediated phase transformation in room temperature grown TiO_2 thin films with enhanced photocatalytic activity
Applied Physics Letters **113**, 084103 (2018); 10.1063/1.5040916
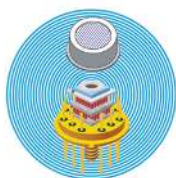
Carbon doping controlled thermoluminescent defect centers in nanoporous alumina for ion beam dosimetry

S. Bhowmick,[1] S. Pal,[1] D. Das,[1] V. K. Singh,[2] S. A. Khan,[3] R. Hübner,[4] S. R. Barman,[2] D. Kanjilal,[3] and A. Kanjilal[1,a)]

[1]*Department of Physics, School of Natural Sciences, Shiv Nadar University, NH-91, Tehsil Dadri, Gautam Buddha Nagar, Uttar Pradesh 201314, India*
[2]*UGC-DAE Consortium for Scientific Research, Indore, Madhya Pradesh 452 001, India*
[3]*Inter-University Accelerator Centre, Aruna Asaf Ali Marg, New Delhi 110067, India*
[4]*Helmholtz-Zentrum Dresden-Rossendorf, Bautzner Landstrasse 400, 01328 Dresden, Germany*

The flexibility of amorphous anodized alumina (AAO) in developing radiation dosimeter for hadron therapy is reported by controlled carbon ion implantation, followed by thermoluminescence (TL) measurements. The efficacy of amorphous AAO in controlling TL sensitivity is found to be governed by an increase in F^+ defect centers as a function of carbon concentration, as revealed from the close resemblance of the trend in photoluminescence intensity. Moreover, its nanoporous structure is demonstrated to be advantageous for defect engineering due to the increase in the surface-to-volume ratio. Detailed X-ray photoelectron spectroscopy analysis suggests the formation of F^+ centers by substituting Al^{3+} ions with C^{2+} in the vicinity of oxygen vacancies, where depth-dependent study showed the evolution of conducting channels owing to sp^2 hybridized C–C bonding, leading to a differential charging effect. This work provides a direction to tune nanoporous AAO in its amorphous form for future ion beam dosimetry. *Published by AIP Publishing.*
https://doi.org/10.1063/1.5050246

I. INTRODUCTION

Anodized aluminium oxide (AAO) in amorphous form with porous structure has widely been investigated because of its innumerable applications as templates, filters, plasmonic devices, optoelectronic devices, bio sensors, and many more.[1–5] The horizon of research using AAO can be extended further to fabricate reliable nanoscale ion beam dosimeter as the use of ion beam is continuously increasing for the treatment of cancer and tumours in hadron therapy.[6,7] Although most of the alumina (Al_2O_3)-based radiation dosimetry studies have been carried out either by using polycrystalline pellets or single crystals,[8–10] amorphous AAO has several advantages over them, like industry friendliness, cost effectiveness, and above all design flexibility either by controlling structure and/or defects induced radiation sensitivity of the active materials.[6,11]

Insulating Al_2O_3 has been studied extensively so far owing to its suitability in radiation dosimetry in the presence of stable trap centers and recombination centers (RCs) within the large bandgap.[12] The working principle relies on the capture of electrons and holes in the trap centers after the exposure to ionizing radiation, followed by the emission of thermally[13] or optically stimulated light[14,15] via recombination of the de-trapped electron-hole pairs in RCs,[13,16,17] while the intensity of emitted light gives a quantitative measure of ionizing radiation. In this respect, carbon-doped alumina $(Al_2O_3:C)$ has attracted much attention not only for

understanding the underlying mechanism but also for improving the radiation sensitivity[6,14,18] where the carbon plays a crucial role in the formation of F^+ centers (i.e., one electron in oxygen vacancy V_O), acting as RCs in radiation dosimetry. But experimental evidence of carbon doping induced controlled evolution of F^+ centers and the related chemistry is scarce in the literature, though inspired by the previous experimental findings, a few groups have recently performed theoretical calculations to explain the mechanism. For instance, Akselrod *et al.*[19] experimentally found the substitution of Al^{3+} by C^{2+} during the growth of $Al_2O_3:C$, leading to the formation of hole trapping centers. They also showed an upsurge in the intensity of the F^+ related absorption with increasing carbon concentration, reflecting the role of F^+ centers as charge compensators with C^{2+} doping. Using positron annihilation spectroscopy, Muthe *et al.*[20] demonstrated that the aluminium vacancies (V_{Al}) decorated with C can lead to the formation of dosimetry traps. Another experimental work by Yang *et al.*[21] also observed a variation of F^+ centers related absorption with carbon doping, though they proposed different mechanisms considering the evolution of V_O by replacing O^{2-} with C^{4-} during the growth process. Furthermore, theoretical works by Choi *et al.* reported that the carbon atoms prefer to sit in the Al sites of alumina,[22] whereas Zhu *et al.* showed that C favours Al sites only when the alumina is O-rich, otherwise they prefer O sites.[23] Similarly Tailor *et al.* theoretically demonstrated that C not only occupies Al sites, but also it moves to those sites in which three-fold coordination with nearest O forms closed-*sp* hybridized C–O bonds, and in turn plays a key role in charge trapping.[24]

---
a)Author to whom correspondence should be addressed: aloke.kanjilal@snu.edu.in

In this article, we discuss the evolution of TL-active F^+ centers in nanoporous amorphous AAO with controlled carbon doping by ion implantation and explore the possibility to use it in radiation dosimetry. Combined XPS and PL measurements, however, confirm the formation of F^+ centers by substituting Al^{3+} sites with C^{2+} in the vicinity of oxygen vacancy. Such active F^+ centers act as recombination sites, and in turn are responsible for controlling TL response. Depth-dependent XPS results further reveal the participation of a fraction of carbon in forming conducting channels and so the origin of a differential charging effect at the C 1*s* core level.

II. EXPERIMENTAL

AAO layers have been prepared by electrochemical etching of highly pure 0.1 mm thick aluminium (Al) foil (99.99%) in the one step process.[25] Initially, an Al foil (area $1 \times 1 \, cm^2$) was anodized in 0.3M oxalic acid at a constant voltage of 30 V for 30 min, where copper has been taken as the cathode. Prepared AAO layers were further dipped into 0.5M phosphoric acid (H_3PO_4) for 30 min. They were finally rinsed in deionized water and annealed at 500 °C in air for 1 h to remove the physisorbed water.[26]

The formation of porous AAO layers was confirmed by scanning electron microscopy, SEM (TESCAN MIRA II LMH), while energy-dispersive X-ray spectroscopy (EDXS) was employed to follow the elemental properties. The depth-dependent compositional analysis was carried out by Rutherford backscattering spectroscopy with a 1.7 MeV $^4He^+$ beam, showing an improvement in stoichiometry with increasing depth (not shown). Grazing-incidence X-ray diffraction (GIXRD) measurements were performed to examine the structural evolution, showing the amorphous nature of AAO (see Fig. S1, supplementary material). Carbon was incorporated in AAO by implanting 50 keV negative carbon ion beam at room temperature (RT) with a fluence in the range of $(0.04–1.3) \times 10^{16}$ ions/cm^2. Note that during ion implantation, ion loses energy by two processes, called nuclear energy loss (S_n) and electronic energy loss (S_e). Such S_n is responsible for substitution of host atoms by the dopant (here, carbon) and creating defects, whereas S_e takes part in the ionization process.[27] Moreover, the negative carbon ion beam avoids charging of AAO surface during ion implantation. The pristine AAO will be referred to hereafter as Q_0 while samples implanted with ion fluence of 4.7×10^{15} (1 at. %), 9.3×10^{15} (2 at. %), and 1.3×10^{16} (3 at. %) ions/cm^2 will be called as Q_1, Q_2, and Q_3, respectively. Prior to C ion implantation, the Stopping and Range of Ions in Matter (SRIM) calculations have been carried out to extract the penetration depth and doping concentration.[27] Detailed microstructural investigation was conducted by transmission electron microscopy (TEM) in cross-sectional geometry by means of a FEI Titan 80-300 microscope operated at an accelerating voltage of 300 kV. Qualitative atomic number contrast imaging based on high-angle annular dark-field scanning TEM (HAADF-STEM) and spectrum imaging based on EDXS were performed at 200 kV with a FEI Talos F200X microscope. TEM lamellae of AAO layers were

prepared by *in situ* lift-out using a Zeiss Crossbeam NVision 40 system. To protect the porous sample surface, a Pt-based cap layer was deposited in the beginning with electron beam assisted and subsequently, Ga focused ion beam (FIB) assisted precursor decomposition. Depth-dependent chemical analyses were carried out by XPS using a monochromatic Al-K_α radiation source ($h\nu \approx 1453.6 \, eV$), where the photoelectrons emitted from the sample surface were analysed by a R4000 electron analyzer of radius 200 mm from Scienta GmbH with an energy resolution of ~0.3 eV at a pass energy of 100 eV. The binding energy (BE) scale with respect to the measured kinetic energy was calibrated from the gold Fermi edge. Depth-dependent XPS measurements have been performed by sputtering with 1.5 keV Ar$^+$ ions. PL was monitored at RT in a Horiba Fluorolog-3 Spectrofluorometer using 325 nm excitation line of a 450 W xenon lamp. The TL signals were recorded in a Harshaw 3500 Reader with a heating rate of 5 °C/s up to a maximum temperature of 400 °C.

III. RESULTS AND DISCUSSION

The porosity of the electrochemically prepared AAO layers was initially verified by top-view SEM as the one documented in Fig. 1(a). As discerned, the footprint of the pores is almost circular (dark contrast) with an average diameter of ~60 nm, as expected for the one-step anodization process.[28,29] However, the corresponding EDXS results reveal the existence of aluminium (35 at. %) and oxygen (63 at. %) along with a feeble amount of phosphorus residue (2 at. %) coming from H_3PO_4, which was used for sample preparation. Bright-field TEM further confirms the formation of a porous layer, where the trenches were found to extend up to ~2 μm below the surface [Fig. 1(b)]. The microstructural properties of the porous AAO layers before and after C ion implantation have been examined by HAADF-STEM imaging too.[30,31] A typical HAADF-STEM micrograph for Q_3 is displayed in Fig. 1(c) showing clear pore formation. Furthermore, EDXS analysis was done within a sub-surface region of ~$1 \times 1 \, \mu$m^2 [indicated by the yellow box in Fig. 1(c)]. The EDXS mappings at the Al and O K-edges, as evidenced in Figs. 1(d) and 1(e), respectively, support the distribution of Al and O throughout the framework of the porous layer. Since C is detected along with Pt in the top layer, it is, therefore, difficult to separate out the implanted C [as expected from SRIM calculation, shown in Fig. 1(f)] from that of the C-containing Pt precursor.

In order to understand the chemical interaction of the carbon with the AAO matrix, detailed depth-dependent XPS measurements were carried out at RT by Ar$^+$ ion sputtering. Figure 2(a) displays the C 1*s* core level spectra of the un-doped AAO by increasing sputtering time. Here, the C1*s* peak was found to be significantly shifted to the higher BE region by ~16 eV, reflecting the highly insulating nature of the porous AAO layers. This leads to a similar peak shift in the Al 2*p* and O 1*s* core levels (not shown) and thus confirms the charging effect.[32,33] Here, the sources of carbon could be from the chemicals used in electrochemical etching[34–36] as well as the adsorption of hydrocarbons under
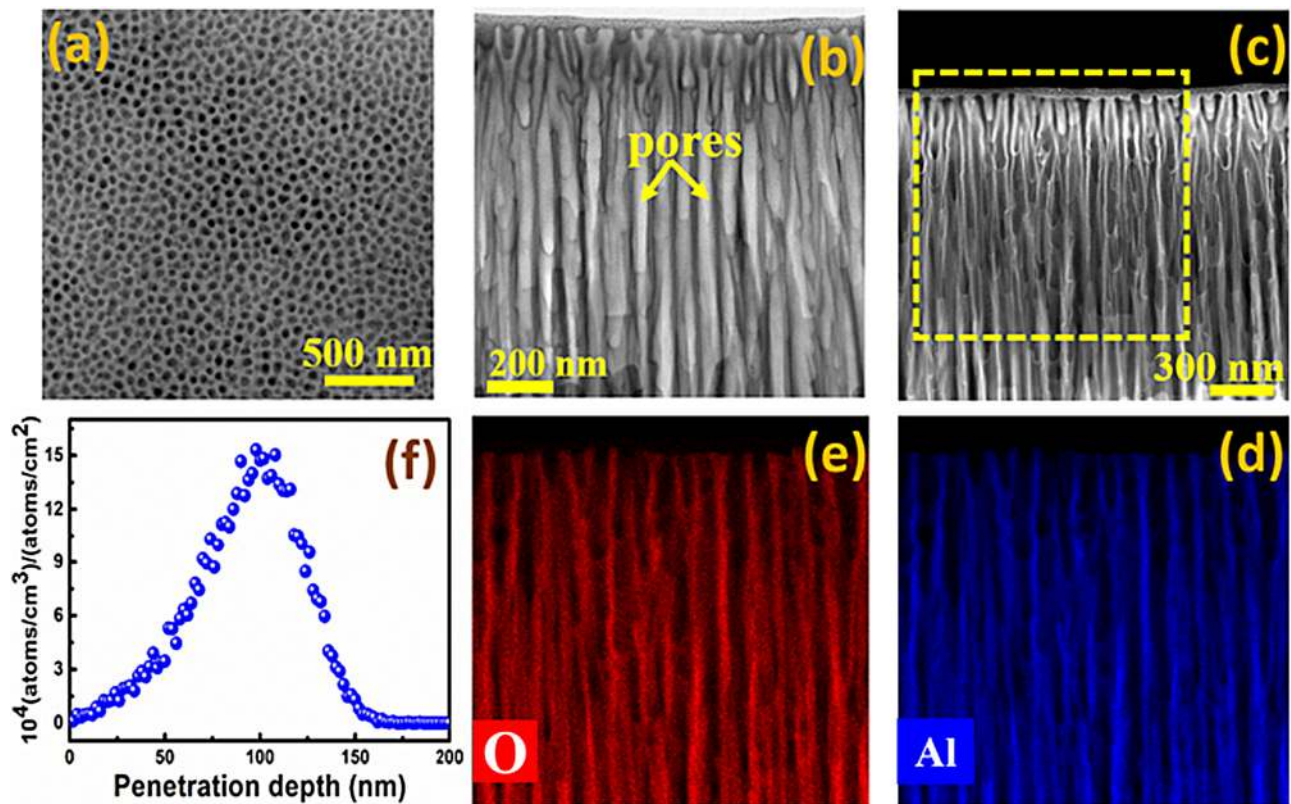
FIG. 1. (a) Representative top-view SEM image of an as-grown AAO layer with an average pore size of ~60 nm; cross-sectional bright-field TEM (b) and HAADF-STEM (c) images of Q_3 display the formation of trenches with an average length on the order of ~2 μm. Spectrum imaging based on EDXS shows that the framework of the porous layer consists of Al (d) and O (e). The SRIM calculation result displays the C distribution in alumina (f).

ambient conditions. However, reduction of the C1s peak intensity along with ~1.12 eV shift towards high BE region after Ar$^+$ ion sputtering indicates the anchoring of carbon atoms in highly stoichiometric alumina deep inside the insulating AAO layer (discussed above). In fact, post anodization annealing at 500 °C is expected to provide a better

attachment of C in the AAO matrix as the one demonstrated by Guenette *et al.*[37]

Interestingly, C implantation with a fluence of 1.3×10^{16} ions/cm^2 (Q_3) also depicts a large shift in C 1s peak position, though another component situated at 284.6 eV has been detected too [Fig. 2(b)]. Similar splitting of C 1s peak
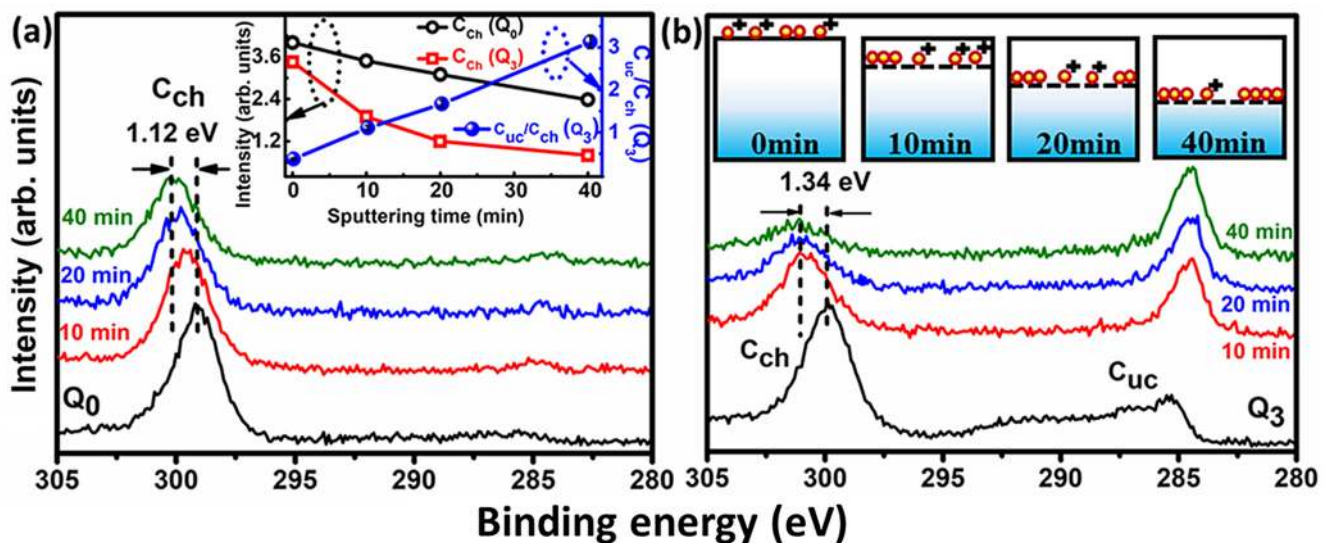
FIG. 2. High-resolution C 1s core level spectra of (a) un-doped AAO (called Q_0) by increasing sputtering time, and (b) after carbon ion beam implantation with a fluence of 1.3×10^{16} ions/cm^2 (Q_3). Inset of (a) represents the variation of C_{ch} and C_{uc} peak intensities, while the inset of (b) depicts a schematic diagram representing the depth-dependent involvement of carbon in realizing differential charging effect. Solid spheres with positive sign indicate charged carbon.
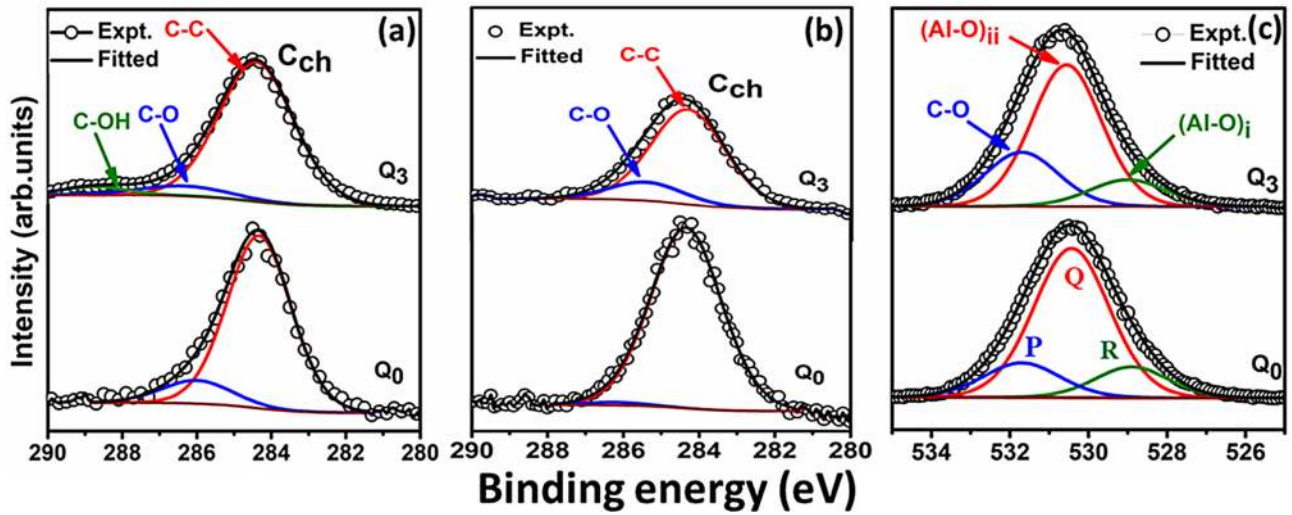
FIG. 3. Deconvoluted charged C-1s (C_{ch}-1s) peak after shifting to 284.6 eV before (a) and after 10 min sputtering (b) for both Q_0 (bottom panels) and Q_3 (top panels). The experimental data and fitted curves are shown by open circles and thick black lines, respectively. The background subtraction curves are also shown in brown, while the deconvoluted components for C–C, C–O, and C–OH are highlighted by red, blue, and olive colours, respectively. Deconvoluted charged O-1s peak after shifting as like in case of C-1s (c), but after 10 min. sputtering for both Q_0 (bottom) and Q_3 (top).

has been found in Al_2O_3 by Bhattacharya *et al.*[33] Simultaneous emergence of two C 1s peaks from the C ion implanted AAO is an indication of non-uniform charging of the matrix during XPS measurements, called *differential charging.*[38,39] Here, non-uniform charging as seen from C 1s spectra is due to the presence of two types of carbon atoms. While one creates bonds in highly insulating AAO, other takes part in developing conducting channels. An increasing trend in C_{uc}/C_{ch} with sputtering time may be a good indicator of channel formation by C ions only, mainly by sp^2 hybridized C–C bonding.[40] Hereafter, the C 1s peak originated from the charged region will be marked as C_{ch} (300 eV) and another as C_{uc} (284.6 eV) for clarity. It is worthwhile to mention that the differential charging effect has only been observed in the C 1s level, but not in Al 2p and O 1s, signifying that the Al and/or O-vacancy did not participate in the formation of conducting channels. Moreover, analysis of the Al 2p core-level spectrum implies the absence of Al–C bond formation[41] (see Fig. S2). Close inspection of the C 1s spectra [Fig. 2(b)] however shows a monotonic decrease in C_{ch} peak intensity, in addition to a peak shift toward high BE region by ~1.34 eV with increasing sputtering time up to 40 min. Nevertheless, an increase in C_{uc} peak intensity has been recorded with sputtering time, and that becomes prominent from the C_{uc}/C_{ch} peak intensity ratio [inset, Fig. 2(a)]. This observation could be a signature of a systematic increase in the conducting channels in the subsurface region that extend through the bulk of the material providing a conducting path so that the charging effect is nullified. Thus, conducting paths form instead of bonding with Al and/or O, with increasing carbon concentration up to the projected range of carbon ions, as revealed from SRIM calculations [Fig. 1(f)]. A broad shoulder near 284.6 eV from the surface contaminants in C-doped AAO disappears due to sputtering [Fig. 2(b)].

To know the nature of the interaction of C atoms with alumina network, detailed analysis of C_{ch} has been carried

out by de-convoluting the C 1s peak after shifting it to 284.6 eV for both pristine and implanted AAO layers. The de-convoluted peak before (a) and after 10 min sputtering (b) in pristine AAO (bottom panel), and the corresponding analysis in C-implanted one (top panel) are shown in Fig. 3.

The C ion implanted sample can be de-convoluted into three components representing C–C (284.5 eV), C–O (286.2 eV), and C–OH (288.2 eV) bonds.[42,43] However, the surface became contamination free after 10 min of sputtering, and in turn it was possible to identify the existence and increase in C–O bonding in implanted samples, as compared with its unimplanted counterpart [Figs. 3(a) and 3(b)]. However, C1s spectra of the implanted sample do not show any signature of Al–C bonding too[41] as has been realized from Al 2p spectra (mentioned above). The enhancement in C–O bonding in case of implanted AAO layers has further been confirmed by deconvoluting the O1s spectra using conventional fitting procedure with Voigt function (after shifting) into three components peaking at about 531.7 eV (P), 530.5 eV (Q), and 529 eV (R) for both pristine and implanted AAO layers after 10 min sputtering [Fig. 3(c)]. The complete fitting results are summarized in Table I. The components P and Q can be attributed to chemisorbed oxygen: The former

TABLE I. XPS fitting components and corresponding binding energies of the O-1s peak before and after C⁻-ion implantation. Within the de-convoluted components, (Al–O)$_i$ and (Al–O)$_{ii}$ represent two different charge states of Al–O bonds for O^{2-} and O^{x-} ($x < 2$).

Sample	Composition	Binding energy ± 0.2 (eV)	Relative percentage (%)
Q_0	(Al–O)$_i$	529.0	16.3
	(Al–O)$_{ii}$	530.5	69.6
	C–O	531.7	14.1
Q_3	(Al–O)$_i$	529.0	13.0
	(Al–O)$_{ii}$	530.5	61.8
	C–O	531.7	25.1
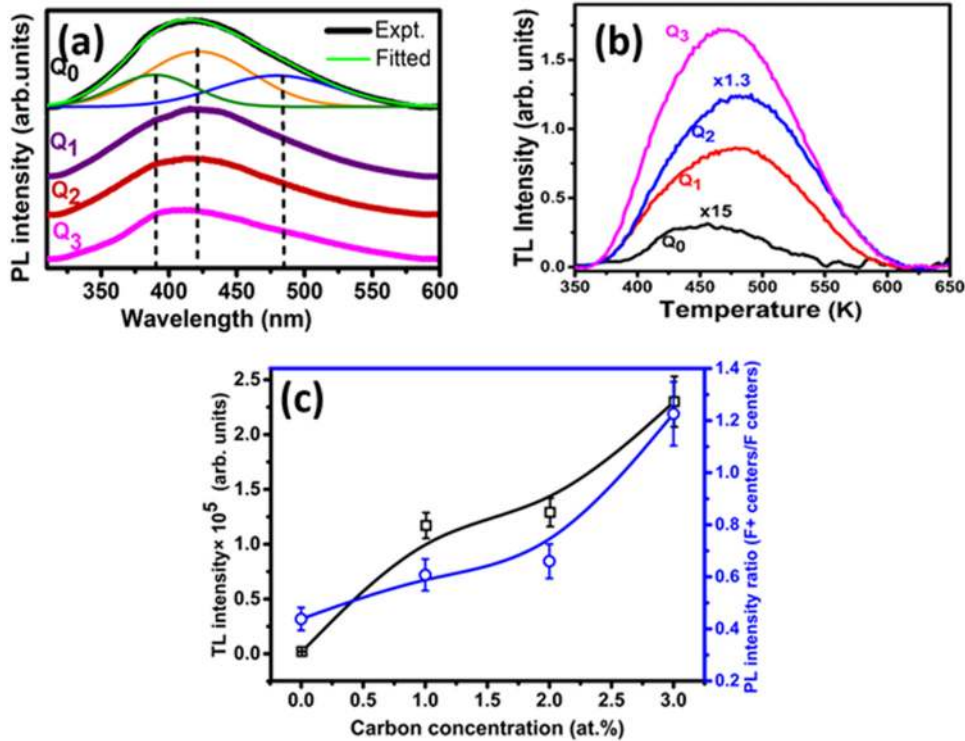
FIG. 4. (a) The PL spectra recorded at RT for both pristine (Q_0) and implanted (Q_1, Q_2, and Q_3) samples. The PL spectra deconvoluted by three Gaussian peaks, where the representative components of Q_0 are superimposed for clarity. Typical TL glow curves of all these samples like Q_0 to Q_3 are exhibited in (b), showing a bell-like feature with a peak at ~470 K. (c) TL response and PL intensity ratio between F^+ centers and F centers as a function of C concentration showing similar trends implying the direct correlation between the F^+ centers and carbon incorporated.

can be assigned to oxygen in C–O and the latter one can be ascribed to O^{2-} ions in the alumina matrix due to the formation of Al–O bonds.[42,44] However, the assignment of R is not straightforward. An increase in peak intensity of P with a systematic reduction for both the components Q and R after carbon ion implantation (Table I) indicates the involvement of O^{x-} ions ($x \leq 2$) for the latter two peaks, and it is most probably associated with the substitution of Al sites by carbon. Here, the contribution of OH^- groups at P can be neglected as the AAO layers have been implanted in high vacuum, and further degassed in UHV atmosphere before XPS measurements. Taking the above observations into account, it seems that both Q and R peaks are associated with Al–O bonds, while the later one is governed by the differential charging due to local differences in the charge state[45,46] in the presence of nearby carbon atoms.

All the previously mentioned theoretical predictions, especially the work reported by Tailor *et al.*, are significant in relation to the present experimental findings, which show an increase in C–O bonding after the incorporation of C in O-rich AAO (discussed above). In this scenario, the formation of active defect centers can be due to the occupancy of C in Al sites and the subsequent formation of C–O bonds in the vicinity of V_O. Now the correlation between the development of C–O bonds and the F^+ centers by C ion implantation in porous AAO layers needs to be explored. To confirm this, initially, PL measurements have been employed at RT, where the recorded spectra are depicted in Fig. 4(a). The typical PL spectrum of the unimplanted AAO can be de-convoluted in three components peaking at ~385, 420, and 480 nm, which are assigned to be the radiative transitions at F^+ centers (i.e., occupancy of one electron in V_O), F centers (two electrons in V_O)[47] and impurities of oxalic acid,[48,49] respectively. However, a clear blue shift of the PL spectra has been

observed with increasing ion fluence, revealing a gradual evolution of the F^+ centers. This is due to the stabilization of more and more F^+ centers as a function of ion fluence by substituting Al^{3+} ions with C^{2+} in the vicinity of V_O,[19,23] in good agreement with the aforementioned XPS results.

Now, to confirm the presence of active F^+ centers, TL has been employed as this is a powerful technique to evaluate the recombination of trapped electron-hole pairs in the recombination centers.[6,13,19,50] Figure 4(b) shows a typical glow curve with a single peak centered at ~470 K indicating the involvement of F and/or F^+ centers.[13] A very weak TL response at a lower peak temperature has been observed in pristine samples, indicating the trapping of electrons/holes during sample preparation. Furthermore, a systematic increase in TL response with increasing C concentration [left ordinate, Fig. 4(c)] has been found and thus showing a possibility to use in ion beam dosimetry. To reveal the involvement of C in stabilizing F^+ centers, the PL intensity (area under the curve) ratio of F^+ and F centers [extracted from deconvolution of PL peaks of Fig. 4(a)] are plotted with increasing carbon concentration [see the right ordinate, Fig. 4(c)]. As discerned, a clear resemblance between the TL and PL responses and thus confirming the direct correlation between F^+ defect centers and the doped carbon, in agreement with previous reports.[19]

IV. CONCLUSIONS

In conclusion, the controlled incorporation of carbon (C) by the ion implantation method and its role in the formation of thermoluminescence (TL) active F^+ centers in nanoporous amorphous AAO have been reported. Detailed XPS analysis revealed the physics behind the C induced formation of F^+ centers which was attributed to be originated by substitution of Al^{3+} ion by C^{2+} ion in the vicinity of V_O in insulating

AAO matrix. This was reflected in the TL response and was further supported by PL results at room temperature. Moreover, differential charging induced C $1s$ peak splitting of $\sim$16 eV at a fluence of 1.3×10^{16} ions/cm^2 due to the development of conducting channels has also been observed, indicating the formation of sp^2 hybridized C–C bonding. Hence, the present results are the benchmark for developing amorphous AAO based ion beam dosimeter by controlled C ion implantation.

SUPPLEMENTARY MATERIAL

See supplementary material for (1) GIXRD patterns of Al foil and 500 °C annealed AAO and (2) high-resolution Al-2p core level XPS spectra of Q$_0$ and Q$_3$ samples.

ACKNOWLEDGMENTS

[1] A. Waleed, M. M. Tavakoli, L. Gu, Z. Wang, D. Zhang, A. Manikandan, Q. Zhang, R. Zhang, Y.-L. Chueh, and Z. Fan, Nano Lett. **17**(1), 523 (2016).

[2] T. Takahashi, R. Tanimoto, T. Isobe, S. Matsushita, and A. Nakajima, J. Memb. Sci. **497**, 216 (2016).

[3] S. Krishnamoorthy, S. Krishnan, P. Thoniyot, and H. Y. Low, ACS Appl. Mater. Interfaces **3**(4), 1033 (2011).

[4] M. M. Rahman, L. F. Marsal, J. Pallarès, and J. Ferré-Borrull, ACS Appl. Mater. Interfaces **5**(24), 13375 (2013).

[5] K. Hotta, A. Yamaguchi, and N. Teramae, J. Phys. Chem. C **116**(44), 23533 (2012).

[6] W. M. De Azevedo, G. B. De Oliveira, E. F. da Silva, , Jr, H. J. Khoury, and E. F. Oliveira de Jesus, Radiat. Prot. Dosimetry **119**(1–4), 201 (2006).

[7] J. Krimmer, G. Angellier, L. Balleyguier, D. Dauvergne, N. Freud, J. Hérault, J. M. Létang, H. Mathez, M. Pinto, and E. Testa, Appl. Phys. Lett. **110**(15), 154102 (2017).

[8] M. S. Akselrod, V. S. Kortov, D. J. Kravetsky, and V. I. Gotlib, Radiat. Prot. Dosimetry. **33**(1–4), 119 (1990).

[9] M. C. Aznar, C. E. Andersen, L. Bøtter-Jensen, SÅJ Bäck, S. Mattsson, F. K-Kristoffersen, and J. Medin, Phys. Med. Bio. **49**(9), 1655 (2004).

[10] J. C. R. Mittani, A. A. R. Da Silva, F. Vanhavere, M. S. Akselrod, and E. G. Yukihara, Nucl. Instrum. Methods B **260**(2), 663 (2007).

[11] J. F. S. Bitencourt and S. H. Tatumi, Phys. Proc. **2**(2), 501 (2009).

[12] E. G. Yukihara, V. H. Whitley, S. W. S. McKeever, A. E. Akselrod, and M. S. Akselrod, Radiat. Meas. **38**(3), 317 (2004).

[13] S. W. S. McKeever, *Thermoluminescence of Solids.* (Cambridge University Press, 1988).

[14] L. B. Jensen, N. A. Larsen, B. G. Markey, and S. W. S. McKeever, Radiat. Meas. **27**(2), 295 (1997).

[15] E. G. Yukihara, E. M. Yoshimura, T. D. Lindstrom, S. Ahmad, K. K. Taylor, and G. Mardirossian, Phys. Med. Biol. **50**(23), 5619 (2005).

[16] S. W. S. McKeever, M. S. Akselrod, L. E. Colyott, N. A. Larsen, J. C. Polf, and V. Whitley, Radiat. Prot. Dosimetry **84**(1–4), 163 (1999).

[17] T. Kato, N. Kawano, G. Okada, N. Kawaguchi, and T. Yanagida, Radiat. Meas. **107**, 43 (2017).

[18] S. V. Zvonarev, V. S. Kortov, T. V. Shtang, D. V. Ananchenko, and K. A. Petrovykh, Appl. Radiat. Isot. **95**, 44 (2015).

[19] M. S. Akselrod, V. S. Kortov, D. J. Kravetsky, and V. I. Gotlib, Radiat. Prot. Dosimetry **32**(1), 15 (1990).

[20] K. P. Muthe, K. Sudarshan, P. K. Pujari, M. S. Kulkarni, N. S. Rawat, B. C. Bhatt, and S. K. Gupta, J. Phys. D Appl. Phys. **42**(10), 105405 (2009).

[21] X. B. Yang, H. J. Li, Q. Y. Bi, Y. Cheng, Q. Tang, and J. Xu, J. Appl. Phys. **104**(12), 123112 (2008).

[22] M. Choi, J. L. Lyons, A. Janotti, and C. G. Van de Walle, Appl. Phys. Lett. **102**(14), 142902 (2013).

[23] J. Zhu, K. P. Muthe, and R. Pandey, J. Phys. Chem. Sol. **75**(3), 379 (2014).

[24] H. D. Tailor, J. L. Lyons, M. Choi, A. Janotti, and C. G. Van de Walle, J. Vac. Sci. Tech. A **33**(1), 01A120 (2015).

[25] H. Masuda and K. Fukuda, Science **268**(5216), 1466 (1995).

[26] H. Hashimoto, K. Yazawa, H. Asoh, and S. Ono, J. Phys. Chem. C **121**(22), 12300 (2017).

[27] J. F. Ziegler, M. D. Ziegler, and J. P. Biersack, Nucl. Instrum. Methods B **268**(11–12), 1818 (2010).

[28] W. B. Yang, Y. L. Zhou, X. H. Tang, B. J. Zhang, and G. Lei, J. Exp. Nanosci. **2**(3), 207 (2007).

[29] G. E. J. Poinern, N. Ali, and D. Fawcett, Materials **4**(3), 487 (2011).

[30] C. M. Brooks, L. F. Kourkoutis, T. Heeg, J. Schubert, D. A. Muller, and D. G. Schlom, Appl. Phys. Lett. **94**(16), 162905 (2009).

[31] T. Walther, J. Microsc. **221**(2), 137 (2006).

[32] D. Briggs and M. P. Seah, *Practical Surface Analysis: by Auger and X-ray Photoelectron Spectroscopy* (Wiley, 2003).

[33] A. K. Bhattacharya, D. R. Pyke, R. Reynolds, G. S. Walker, and C. R. Werrett, J. Mat. Sci. Lett. **16**(1), 1 (1997).

[34] G. S. Huang, X. L. Wu, L. W. Yang, X. F. Shao, G. G. Siu, and P. K. Chu, Appl. Phys. A **81**(7), 1345 (2005).

[35] I. Vrublevsky, K. Chernyakova, A. Ispas, A. Bund, N. Gaponik, and A. Dubavik, J. Lumin. **131**(5), 938 (2011).

[36] G. H. Li, Y. Zhang, Y. C. Wu, and L. D. Zhang, J. Phys. Condens. Matt. **15**(49), 8663 (2003).

[37] M. C. Guenette, M. D. Tucker, M. Ionescu, M. M. M. Bilek, and D. R. McKenzie, J. Appl. Phys. **109**(8), 083503 (2011).

[38] S. Suzer, Anal. Chem. **75**(24), 7026 (2003).

[39] J. M. Gorham, W. A. Osborn, J. W. Woodcock, K. C. K. Scott, J. M. Heddleston, A. R. H. Walker, and J. W. Gilman, Carbon **96**, 1208 (2016).

[40] S. K. Jerng, D. S. Yu, J. H. Lee, C. Kim, S. Yoon, and S. H. Chun, Nanoscale Res. Lett. **6**(1), 565 (2011).

[41] B. Maruyama, F. S. Ohuchi, and L. Rabenberg, J. Mat. Sci. Lett. **9**(7), 864 (1990).

[42] K. Shimizu, C. Phanopoulos, R. Loenders, M. L. Abel, and J. F. Watts, Surf. Int. Anal. **42**(8), 1432 (2010).

[43] D. Tang, J. Su, Q. Yang, M. Kong, Z. Zhao, Y. Huang, X. Liao, and Y. Liu, RSC Adv. **5**(68), 55170 (2015).

[44] A. K. Nanda Kumar, S. Prasanna, B. Subramanian, S. Jayakumar, and G. M. Rao, J. Appl. Phys. **117**(12), 125307 (2015).

[45] A. Celebioglu, S. Vempati, C. O. Akgun, N. Biyikli, and T. Uyar, RSC Adv. **4**(106), 61698 (2014).

[46] B. V. Crist, *Handbooks of Monochromatic XPS Spectra* (XPS International, Mountain View, CA, 1999).

[47] W. L. Xu, M. J. Zheng, S. Wu, and W. Z. Shen, Appl. Phys. Lett. **85**(19), 4364 (2004).

[48] Y. Yamamoto, N. Baba, and S. Tajima, Nature **289**(5798), 572 (1981).

[49] X. Wu, S. Xiong, J. Guo, L. Wang, C. Hua, Y. Hou, and P. K. Chu, J. Phys. Chem. C **116**(3), 2356 (2012).

[50] E. G. Yukihara and S. W. S. McKeever, J. Appl. Phys. **100**(8), 083512 (2006).